Supplementary Materials

Methods and Materials

Swabbing protocols for HSV. Study participants performed swabbing of the genital tract. To document viral expansion and decline of mucosal HSV-2 during a genital lesion, participants performed daily swabs until a lesion developed and continued to swab until after lesion healing. Each swab was processed for quantitative polymerase chain reaction (PCR) (*1*). Data included 115 episodes from 81 persons **(SM 1 and 2)**. Participants swabbed the entire anogenital tract for each lesional shedding episode. We used the derived curves for curve-fitting and parameter value estimation.

In another study, 25 participants performed every six-hour anogenital swabs for a total of 60 days to document the nature of asymptomatic and symptomatic genital tract shedding (*2*). We compared this data with our 365-day stochastic model simulations. Of note, in the original manuscript describing shedding patterns in these 25 patients, we used 150 copies of HSV DNA per mL of transport medium as a cut-off for detection. We re-analyzed the data for this study with a new cut off of 50 copies of HSV DNA per mL of transport medium based on an analysis that this is likely to be the cut-off value with the best performance characteristics (*3*).

All study participants signed informed consent. The University of Washington Institutional Review Board approved the study protocol.

Mathematical model: detailed explanation of parameters with respect to HSV-2 biology. We first describe the HSV-2 replication cycle in the genital tract and immunologic response to HSV-2 infected cells with reference to each of our model's parameters. Our model assumes chronic infection rather than acute infection. During the *latent phase* of chronic genital HSV infection, the virus is maintained in a dormant state in the sacral ganglia. During *reactivation*, HSV-2 virions are released from neuronal endings at the dermal-epidermal junction at a certain rate (ϕ). Released virions survive in the genital tract for a defined duration ($1/c$) during which time they can infect local epithelial cells. Viral infectivity ($1/(\beta * S0)$) is roughly defined as the number of viruses that are needed to infect one epithelial cell per day assuming the constant presence of viruses. We observe that if an epithelial cell becomes infected, then it will die either via direct viral lysis if the cell survives long enough to become packed with viruses and lose its function

(lifespan = 1/*a*), or it will die via CD8+ lymphocyte mediated killing (lifespan = 1/(*f**E)). Lymphocyte killing efficiency (*f*) is defined as the number of infected cells cleared by one CD8+ lymphocyte cell per day *in vivo*. If an epithelial cell evades CD8+ lymphocyte mediated killing for the entire duration of cellular infection, it will produce a total of *p/a* viruses: this number represents the burst phase of each infected cell; *p* is defined as the rate of viruses produced by an infected cell per day.

HSV-2 reactivation that results in mucosal HSV shedding can be subclinical or clinical **(fig. S1)**. Clinical shedding is termed a *recurrence* and is classically associated with sporadic crops of vesicles, which form due to the death of closely congregated epithelial cells. Vesicles progress to ulcers and then after about a week undergo healing due to re-growth of susceptible cells: we assume that re-growth occurs according to a growth rate, λ or $d^*(S0 - S)$ with growth limited by S0, the initial number of susceptible cells, which is also the carrying capacity of the system. A group of closely approximated vesicles and / or ulcers is termed a *lesion*. Often an initial crop of closely spaced vesicles or ulcers, or a single vesicle is followed by a group of secondary vesicles in the surrounding region (*4*).

Sub-clinical shedding episodes are common during chronic HSV-2 infection and are defined by local detection of virus either by viral culture or PCR, in the absence of a clinically apparent genital lesion or symptoms. It is not known what proportion of the virus detected during sub-clinical shedding is of neuronal or epithelial origin. However, reactivations are likely to be more frequent than genital ulceration and can occur on multiple occasions during a single ulcer (*5*). Sub-clinical episodes are also typically associated with a lower copy number of HSV (*2*).

The formation of a clinically apparent genital lesion is accompanied by rapid accumulation of localized CD8+ lymphocytes at the dermal-epidermal junction at a peak rate (θ), followed by a slow decay of these cells over a period of at least 5 months after lesion healing (lifespan = $1/\delta$) (*6, 7*). The CD8+ replication rate in our model is saturated at θ, and $\theta/2$ occurs when infected cells are equal in number to parameter *r*, which represents how many epithelial cells need to be infected prior to half-maximal CD8+ expansion. Therefore, parameter *r* defines how rapidly immune cells recognize and respond to viral antigens on the surface of infected cells.

Detailed explanation of model curve fitting. We used **Berkeley Madonna Version 8.3.18** to numerically solve our series of ordered differential equations. The Euler's method of integration

was employed with a step size of 0.001 days (*8*). We used Madonna's curve fitter option to establish a set of parameter estimates for each curve. The Madonna curve fitter uses nonlinear least-squares regression that minimizes the sum of the squared residuals between experimental and predicated data of HSV copy number. We weighted the data points equally for our fitting procedure. The curve fitter asks for minimum and maximum estimates for each parameter: we derived these value ranges from detailed review of the literature as described below. The curve fitter also asks for two initial parameter estimates to initiate simulations: we included values at approximately 25% and 75% values between the minimum and maximum as our initial estimates.

We solved our equations for eight parameters: viral infectivity (β), infected cell lifespan ($1/a$), viral production rate by epithelial cells (p), viral lifespan ($1/c$), CD8+ lymphocyte expansion rate (θ), CD8+ antigen recognition (r), initial CD8+ density ($E0$) and CD8+ killing efficiency (f). We also attempted to solve our model with only four parameters (β, $1/a$, p and $1/c$) in a subset of 20 curves. Two parameters, CD8+ mucosal lifespan ($1/\delta$) and neuronal viral production rate (ϕ) were not included in any curve fitting because the effect of these parameters is demonstrated in the model only over a longer duration of time rather than during an individual shedding episode.

Detailed description of inclusion and exclusion criterion for patient-derived shedding curves. Patient curves were excluded for missing data points and for non-monotonic decline in virus that is likely to be associated with secondary crops of vesicles. Secondary crops of vesicles occur in about 45% of lesional shedding episodes and may logically cause non-monotonic decline in shedding curves (*4*). These new vesicles may or may not be contiguous to the initial set and are associated with extension of the lesion and a subsequent increase in viral replication (*4*). To focus on the initial events of mucosal ulceration, we selected the mucosal shedding curves that were likely to be tightly associated with the first set of vesicles or ulcers, and censored those that were likely to be associated with secondary crops of vesicles (defined as a positive rebound of at least one log in viral load). We censored included curves to the last point of viral decline.

We also wished to only include curves that incorporated the full extent of viral expansion and decline from the first crop of vesicles. We therefore eliminated curves in the event of a single missed data point during the first two days of shedding, or when there were no points representing the up-slope or down-slope of an outbreak. In addition, if non-monotonic rebound occurred, then the curve was only included in our analysis if the decline went below 10^4 HSV copies prior to viral rebound.

Anogenital versus lesion only swabs. A concern with the use of anogenital swabs as empiric data is that concurrent shedding in other areas of the genital tract might contribute to the total number of HSV copy number, despite being outside of the small anatomic area of a single lesion that the model is attempting to capture. To validate the use of anogenital swabs for our curve fitting, we compared our data with the concurrent swabs taken only from genital lesions. In 15 of our 89 included episodes, lesion-only swabs were obtained at the same time as anogenital swabs. We performed curve-fitting exercises with the model to curves derived from lesion only swabs, and compared parameter estimates to those derived from anogenital swabs.

Parameter starting values. For our deterministic and stochastic simulations, initial levels of infected cells (I0), virus from neurons (Y0), and viruses from epithelial cells (Z0) were zero. Initial levels of susceptible cells (S0) were 5.4e6: the derivation of this number is described in the section describing model micro-anatomy below.

We used the initial number of CD8+ T-cells (E0) as a fitting parameter for our deterministic curve fitting to patient-derived PCR curves. CD8+ lymphocyte levels are highly dynamic in the genital tract over time in HSV-2 infected persons and persist in the genital tract for at least 5 months after lesion healing (*6, 7*). In our model simulations, E0 at episode initiation inversely correlates with peak HSV copy number of the episode but E0 was not sampled prior to lesion formation in our patients: therefore, it was necessary to use *E0* as a fitting parameter.

For our stochastic simulations, we calculated a separate measure of E0 for each set of patient parameters. While our curve fitting used data from a high-copy episode HSV shedding episode associated with a genital lesion, our stochastic simulations were meant to survey disease activity over a longer period of time, which may or may not include high-copy episodes. We did not assume a low initial CD8+ lymphocyte level for these stochastic simulations because we did not wish to automatically begin each simulation with a high-copy (lesional) episode. We therefore performed an initial 365-day stochastic simulation with each set of parameters, and calculated the mean value of CD8+ lymphocyte levels over this entire 365-day period. To accomplish this, we sampled CD8+ T-cell levels repeatedly at a time step of 0.001 days, summed all of these values and divided the sum by 365000. We generated a separate E0 value for each of the 89-parameter sets used for the stochastic simulations in our paper.

Micro-anatomic description of model area and genital ulcers. Our model recreated a two-centimeter diameter circular area (surface area = 314 mm^2) of susceptible epithelial cells in the anogenital mucosa as the typical maximum size for a single lesion. We chose this diameter because the average surface area of recurrent genital HSV lesions in immunocompetent persons is 60 mm^2 (range 2 – 270 mm^2), which equates to a circular lesion of diameter 8.7 mm (range 1.6 – 18.5 mm) (*4*). Thus, we designed our initial model to be inclusive of the vast majority of recurrent genital ulcerations in immunocompetent persons.

To detect virus from a genital swab rubbed over a mucosal or skin surface, a micro-ulceration must be present during a sub-clinical reactivation. In other words, enough nucleated epithelial cells must die during a reactivation for virus to gain access to the outermost layers of the epidermis. In normal skin, nucleated epithelial cell thickness varies according to variation in depth of the dermal-epidermal border. We reviewed histologic slides from biopsies performed in the genital tract in our study subjects and detected that the thickness of nucleated epidermal cells ranges from between 3 and 20 cells. Assuming that initial cell infection occurs at the dermal-epidermal border, we surmise that at least this many cells must die for viral detection to occur.

We estimated the number of susceptible cells prior to introduction of virus (S0) based on the number of cells that pack into a hypothetical 2 centimeter diameter cylinder with volume equal to height multiplied by area of a circle (*9*). We examined skin biopsies of genital lesions to define the average depth between the peripheral nerve endings and the outermost layer of nucleated, susceptible epithelial cells. To estimate the radius of a single cell on digitized histology slides, we used **Free Ruler 1.7b5** (designed by Pascal Balthrop, Brooklyn, New York, www.pascal.com/software/freeruler/) to measure the diameter of the ten largest *stratum spinosum* cells from a 400 μm wide biopsy of the peri-anal skin**,** averaged these measurements, and divided the mean by two (cell radius = 8.5 μm). To estimate the height of the cylinder of susceptible cells in a two centimeter diameter area of ano-genital skin, and to account for the uneven nature of the dermal / epidermal borders, we took 20 evenly spaced vertical measurements from the dermal / epidermal junction to the bottom of the *stratum lucidum* and then calculated the mean of these numbers. These height measurements were then performed individually on several peri-anal skin histology slides and averaged (74 μm). Similar numbers of cells were predicted whether we assumed cuboidal (4.7e6) or spheroid cell shape (5.4e6). We chose spheroid cell shape for all runs of the model. Calculations are all performed with units of μm:

Assuming spheroidal cell shape:

Initial number of susceptible cells (*stratum spinosum / basale / granulosum*) =

(Volume of susceptible area in genital mucosa / Spheroid cell volume) * adjustment factor for how many spheres fit into a column

adjustment factor for how many spheres fit into a column = 0.64 (*9*)

$[(height*\pi*mucosaradius^2) / (4/3*\pi*cellradius^3)] * 0.64 =$

$[[(74*\pi*10000^2) / (4/3*\pi*8.5^3)] * 0.64 =$

5.4223e6

Assuming cuboidal cell shape:

Volume of susceptible area in genital mucosa / Cuboidal cell volume =

$(height*\pi*radius^2) / (8*cellradius^3) =$

$(74*\pi*10000^2) / (8*8.5^3) =$

4.7318e6

Calculation of lesion diameter. We calculated lesion diameter by subtracting the number of susceptible and infected cells at a certain point in time from the initial number of susceptible cells. The difference in this equation is the number of cells that have been infected and died, but have yet to grow back according to the susceptible cell growth function:

Number of missing cells = 5.4223e6 (i.e total number of cells) - S - I =

Ulcer area / Volume of a cell = $(74* \pi *(R^2)*0.64) / (4/3*\pi*8.5^3)$

where R = radius of an ulcer.

$5.4223e6 - S - I = (74 * \pi * (R\hat{}2) * 0.64) / (4/3 * \pi * 8.5^3)$

Diameter of an ulcer = R * 2

Therefore, **Diameter of an ulcer = $2 * \sqrt{(9.38123e7 - (S+I)/0.0578)}$**

We recalculated diameter at each time step according to the above equation. We defined a recurrence as lesion greater than 2 mm in diameter.

Stochastic model simulations: We converted the deterministic model to a stochastic stage-structured form with unchanged compartmental structure. We used a technique developed in an intra-host model of T-cell response in which equation variables are updated according to serial probability measures at the end of each time-step (Δt = 1.5 minutes) (*10*). Fundamental assumptions of the model are that parameters derived from the curve fitting are unchanged with conversion to a stochastic format, and that these parameters remain intact during and after resolution of a shedding episode. We included constant values for parameters not included in curve fitting (δ=0.05/day, and ϕ=50 HSV copies per day). We chose 50 DNA copies per day for model simulations because this rate produced outcomes of shedding frequency and recurrence consistent with those in the literature.

Stochastic simulations and derivation of neuronal release rate of HSV DNA (ϕ): Realistic lower and upper bounds for neuronal virus production rate (ϕ) were unknown prior to this study. We therefore ran the model with various levels of this parameter initially (1, 2, 5, 10, 25, 50, 100, 200, 1000 and 2000 viruses per day). Values less than 5 viruses per day sometimes resulted in no detectable shedding episodes. Values more than 200 viruses per day resulted in persistent shedding rather than the intermittent, variable shedding episodes that are normative with observed infection in the vast majority of immunocompetent patients with HSV-2 infection. Values between 25 and 100 routinely resulted in clinically relevant outcomes: we therefore selected 50 viruses per day for the majority of our analyses.

Parameter derivation: Viral infectivity (β). β, or rate of infection of susceptible epithelial cells, is defined in our model as the number of DNA copies of genomic HSV-2 needed to infect one

susceptible cell per day assuming the constant presence of viral particles. β can be estimated experimentally by varying the multiplicity of infection or MOI. MOI is defined as the ratio of infectious agents (often termed particle forming units) added to target cells under experimental conditions. The formula $P(n>0) = 1 - e^{-m}$, where m is the MOI, describes the average proportion of cells that will be infected at a particular MOI. It is important to note that MOI refers to infectious particles (rather than a strict count of total particles or total genomic DNA copies per infected cell as used in the definition for β) that are necessary given the varying infectivity of different agents. MOI therefore is a constant regardless of the infectivity of a particular virus, whereas β in our model describes infectivity.

In a published experiment, when Vero cell lines were infected with 20 wild type HSV-1 virions per target cell, approximately 50% of cells displayed viral gene transcription 12 hours after inoculation (*11*). Therefore, introduction of 20 wild-type particles per cell achieved P(n>0)=0.5 and 20 wild-type virions achieved an MOI of 0.693. To generate a hypothetical range of the number of virions per target cell that could initiate infection, we calculated the infectivity that would be needed to infect 10% (MOI=0.11) and 90% (MOI=2.3) of Vero cells under these conditions. The resulting range is 3 to 66 total genomic HSV-2 DNA days per one particle forming unit (Ψ): in other words, if Ψ=50 then the constant presence of 50 DNA particles over the course of a day will result in infection of one cell. β can be derived from these figures at onset of infection via the following formula: $\beta = 1 / (S0 * \Psi)$. The resulting range for β in the peri-anal / buttock region where S0 = 5.4223e6 is **(2.67e-9, 5.87e-8).** This range of values for β led to excellent curve fit on initial curve fitting exercises and therefore, the range was maintained for all subsequent curve fits.

Parameter derivation: Infected cell lifespan (1/a). In cell cultures, an HSV infected cell lives 18-20 hours in the absence of CD8+ mediated cell lysis prior to releasing virions. This allows for a death rate (parameter *a*) with the following lower and upper bounds **(24/20, 24/18) or (1.2, 1.33)**(*12*).

Parameter derivation: Maximal rate of CD8+ lymphocyte expansion (θ). The CD8+ lymphocyte cell expansion phase during viral infection has been characterized by fitting a multi-phasic mathematical model of CD8+ cell expansion, rapid contraction and prolonged contraction to the cellular immune response against 6 different LCMV epitopes in a murine model of LCMV infection. The expansion phase was defined as $dE/dt = \theta T$ where θ is the expansion rate. Values for θ for the 6 epitopes ranged from 1.13 to 1.92 $days^{-1}$ with 95 confidence intervals from 0.98 to

2.21. This equates to a CD8+ doubling time ranging from 7 to 16 hours (*13*). A continuous model of T-cell activation has also been applied to LCMV data where increases in a viral load saturation function over time allow for density dependent CD8+ cell expansion. This is similar to our model, which uses an infected cell saturation function to allow for inclusion of the mass action principal with an inherent upper limit on rate of CD8+ cell expansion. Under the continuous model, the estimate for θ was 2.92 $days^{-1}$ with 95 confidence intervals from 2.74 to 3.1 (doubling time 5 to 6 hours). Given that there is no existing data on CD8+ expansion rate to HSV-2 infected cells in the human host, we employ the widest range of estimates from both of the above LCMV models to obtain lower and upper bounds for values of θ (0.98 to 3.1, i.e. doubling times of 5 to 16 hours).

Parameter derivation: Saturation function of infected cells (r). *r* is the saturation function of infected cells for effector CD8+ cell production. We employ a wide range of 5 to 200 to allow for different thresholds at which CD8+ expansion may occur. A high parameter *r* exists if CD8+ recognition of MHC-peptide presentation by infected cells is sluggish.

Parameter derivation: Efficiency of CD8+ lymphocyte killing (f). Ganusov and colleagues estimated the number of target cells killed by one antigen primed CD8+ T effector cell per day (parameter *f* in our model) by fitting a mathematical model to results generated from a widely used *in vivo* cytotoxicity mouse assay of splenic LCMV infection. In this assay, LCMV peptide-pulsed splenocytes are infused into the bloodstream, and then migrate to the spleen where they are cleared rapidly by CD8+ memory and effector cells (*14*). The estimates, which ranged from an average 0.1 to 2 target cells killed per day by a single CD8+ lymphocyte effector cell in the mouse spleen, are likely to be overestimates for the human mucosal HSV-2 system. First, the spleen is an immunologic organ and is likely to have a higher effector to target cell ratio: during a high titer shedding episode of HSV-2 in the genital tract, this ratio is apt to be much lower and the time for a CD8+ effector cell to locate and engage an infected cell may be longer. Second, when the authors also make a separate type of estimate for the parameter of CD8+ cell killing efficiency by estimating infected cell death rate in unit $hours^{-1}$ during the peak of CD8+ cytolytic response, their estimate is higher than other available estimates in the literature by 1 to 2 logs. A possible reason for this discrepancy is that the newer model assumes a slower rate of migration of target cells from the blood to the spleen. In addition, the epitope density of infused target cells was higher than in other experiments and is unlikely to reflect the epitope density during natural viral infection: not only does HSV-2 interfere with the antigen presentation process of the

infected cell, but CD8+ cells are also likely to encounter HSV-2 infected cells early during infection when the epitope density on the infected cell surface is relatively low compared to that of the infused splenocytes in the LCMV model.

When these high values of parameter *f* are used in our model, the resultant CD8+ levels are unrealistically low compared to our clinical data though all other dynamic measures and parameters of the model remain unchanged (*6, 7*). In fact, increasing parameter *f* has a very isolated effect in our model, which is to lower values of CD8+ cell level before and after a high-copy event. During curve fitting exercises, if ranges of the upper and lower bounds for parameter *f* are increased or decreased substantially, it has only a marginal effect on other parameters estimates. Moreover, adjusting parameter *f* for individual model runs has no effect on the inherent dynamics of the model, and no effect on any of the key outcomes of the model (number of high-copy episodes per year, shedding frequency, or diameter of ulcer). The reason is that CD8+ killing efficiency (*f*) and CD8+ level are entirely dependent on one another to the extent that 1/(*f**T), which determines the lifespan of an infected cell, remains constant with wide adjustments in *f*.

While 1/(*f**T) remains constant with adjustments in *f,* it is currently impossible to know from our experimental data whether our individual estimates for parameter *f*, or for true CD8+ T cell density per two centimeter diameter area are accurate. Though our model incorporates robust estimates of CD8+ cell decay rate in the mucosa (parameter δ), we only have an imprecise view of CD8+ lymphocyte density in a two-centimeter diameter area in the mucosa (the area assumed in the model); this is because our sequential measures of CD8+ infiltration are from a 1-mm^2 area of the biopsy (*6, 7*). It is possible to multiply each CD8+ value by π*(10 $mm)^2$, or 314, to estimate the number of CD8+ cells in that would inhabit a two centimeter diameter area at the dermal-epidermal junction assuming uniform density. Yet, it is doubtful that CD8+ density is uniform throughout this larger area because herpetic ulcers are usually much smaller than two-centimeter in diameter and CD8+ T-cells appear to be exquisitely localized to the micro-environment of infection. Even at sites 2 centimeters away during the acute phase of an ulcer, there is only scant CD8+ infiltration and this is likely to be the case even closer to the ulcer edge. An appropriate parameter *f* value should therefore probably produce peak and trough CD8+ levels that fall somewhere in the range between CD8+ levels in a one-mm^2 area, and our hypothetical estimates of uniform CD8+ density in a 314 mm^2 (two centimeter diameter) area. In the study by Zhu, the average number of CD8+ cells in a 1-mm^2 area was 1244 at peak and 146 at trough (*7*). Assuming uniform density of CD8+ cells in a 1-centimeter diameter area, the corresponding peak and trough CD8+ levels would be 390000 and 45800. To allow our model to accommodate this

fact, and because in other LCMV mouse systems, estimates of the death rate of infected cells were 10 to 100-fold lower than in the previously described murine LCMV model (*15-17*), we chose a range of upper and lower bounds 1 to 2 logs lower (0.001, 0.2) than those derived by Ganusov and colleagues.

Of note, Ganusov's parameter estimates may have important relevance to the human HSV-2 system: approximately 0.1 - 1% of CD8+ cells in the genital mucosa are HSV-2 primed (*7*). Due to increased TCR-peptide avidity, it is possible that the true *f* parameter of this specific population of cells may be considerably higher. However, we chose to look at the average killing rate of all CD8+ cells measured in the mucosa.

Parameter derivation: CD8+ lymphocyte decay rate (δ). The CD8+ lymphocyte decay rate was derived from longitudinal data on 6 patients who had 2 to 7 serial biopsies at sites of healed genital ulcers over periods of 28 to 56 days (*7*). Each patient had their decay curve fit to a simple exponential decay model of $dE/dt = -\delta T$ to generate estimates of parameter δ. The mean of δ for the 6 patients was 0.05 with a range from 0.03 to 0.082 (mean lifespan of 20 days, range of 12 to 33 days). These lower and upper bounds were not used for curve fitting.

Parameter derivation: Virus produced per cell per day (p). *p* is defined as the number of copies of DNA produced by an infected epidermal cell per day. We chose genomic copies rather than infectious virions (particle forming units) because our model is fit to PCR curves that measure concentration of DNA by PCR. Our estimates for *p* were determined from kinetic studies of HSV-1 or 2 viral DNA replication based on single-cycle growth in vivo growth assays. Estimates were generated either by extrapolating genomic copies on growth curves 24 hours after infection and dividing this number by the number of infected cells (*18, 19*), or by multiplying the viral burst size (PFU/cell) by the DNA copies/PFU (*18, 19*). Estimates varied by cell line and assay conditions: the broad range of outcomes is reflected in our lower and upper bounds. Lilley noted a 12000 to 20000 fold amplification of viral DNA at 24 hours: this translates to a upper bound for *p* of 20000 multiplied by 24/18 (26700) because cell death may occur over as short a time as 18 hours. The low bound for DNA production in two studies was 1000 and in one study was 4320. Therefore, our final intervals for viral production were (1000, 26700). As a descriptive measure to describe true per cell burst phase, we use the termpk/a.

Parameter derivation: Free viral lifespan (1/c). *c* is defined as free viral decay rate in the mucosa or in infected cells after being produced by an infected cell. $1/c$ is the free viral lifespan

(i.e. how long a free virus remains infectious prior to denaturing). The upper bound for this value was generated from two sources. First, in a small experiment, free virus did not appear to remain infectious more than two hours after being inoculated on human skin (*20*). Second, more recent shedding protocols in our clinic show that in at least three patients, short bursts of viral shedding lasting less than 2 hours are present. This implies that the average lifespan of the virus is likely less than 2 hours. Because both of these observations are derived from limited patient data, and because our simulations generated persistent rather than sporadic shedding with free viral lifespan of 4 or more hours, we allowed the upper bounds to extend to 3 hours of free viral survival. As lower bounds of viral lifespan, we arbitrarily chose 15 minutes. Therefore bounds for free viral death rate are (24/3, 24/0.25) or (8, 96).

Parameter derivation: Growth function of susceptible cell regeneration during infection (d(S-S0)). Parameter *d* determines how quickly cells regenerate after dying during infection. Realistic estimates for this figure can be obtained from our natural history database where symptomatic lesions persist for a range of 1 to 21 days. Therefore, rate of regeneration can range from (1/21 to 1/1) or (0.05, 1). Given that adjusting this variable has little effect on model dynamics, it was arbitrarily maintained constant at 0.22 $days^{-1}$ or regeneration time of 4.5 days.

Figures

Supplementary Figure 1. Schematic diagram of HSV-2 pathogenesis with viral entry, latency, asymptomatic shedding, and clinical recurrence.

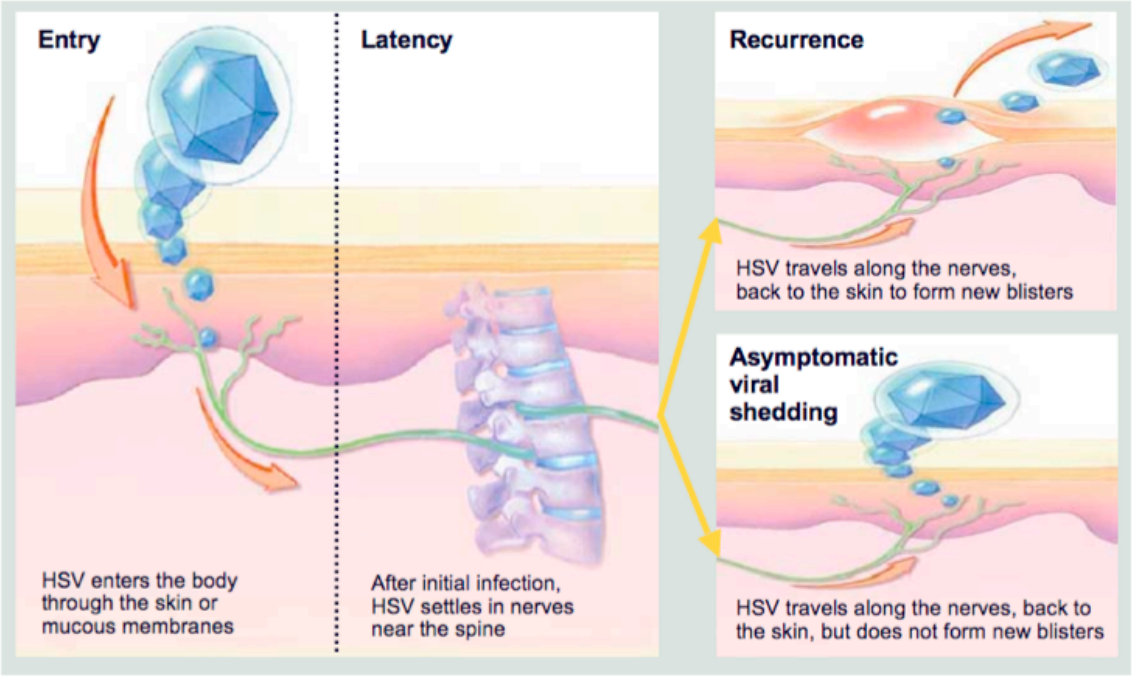

Supplementary Figure 2. The deterministic form of the model with CD8+ lymphocyte parameters achieves good fit with empiric data from lesional swabs. Sixteen examples of deterministic model curve fitting to mucosal HSV-2 shedding curves with daily serial quantitative PCRs performed on anogenital lesions. Actual patient quantitative PCR data from anogenital swabs (blue circles) and lesional swabs (green triangles) performed during lesions, and deterministic model fits (red lines).

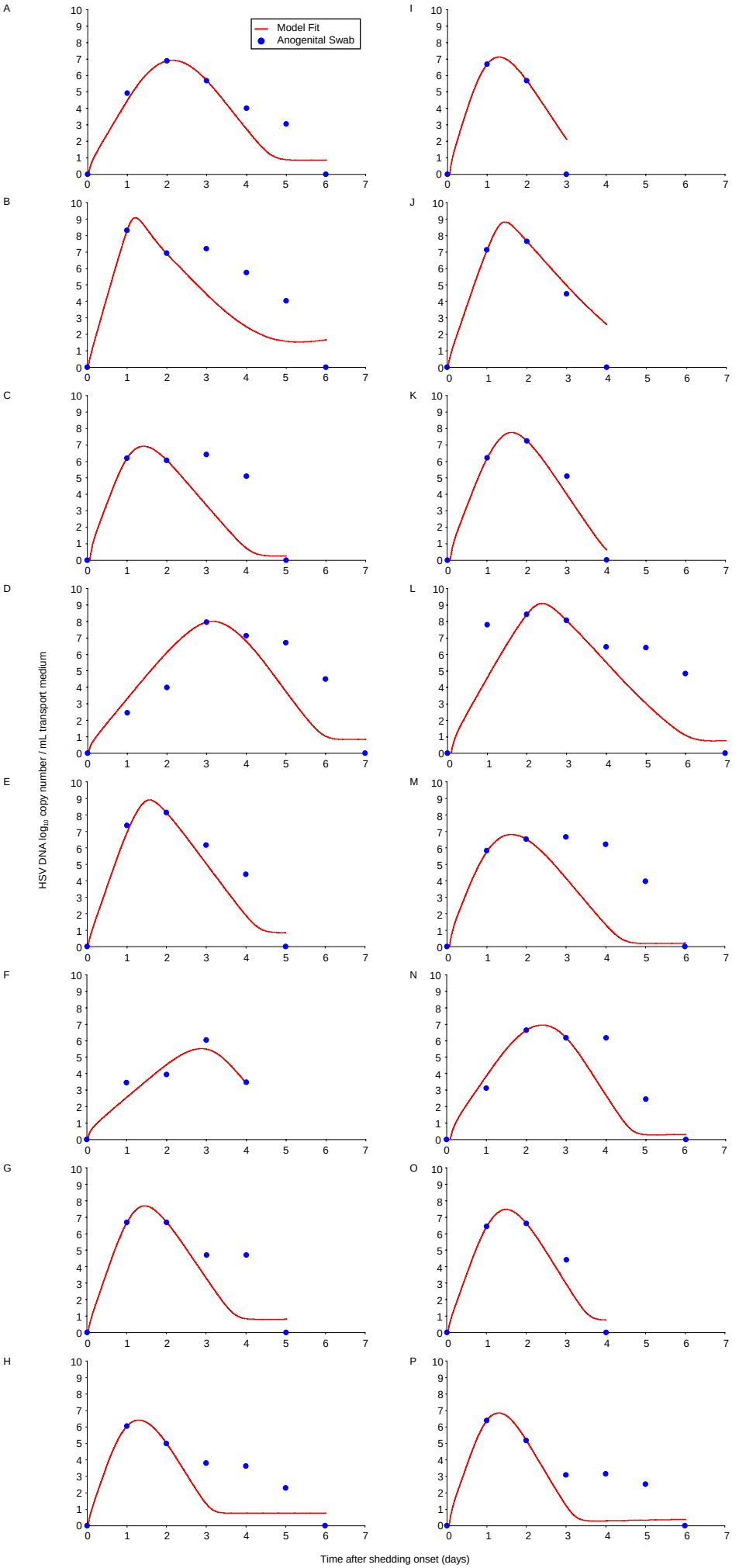
A
B
C
D
E
F
G
H
I
J
K
L
M
N
O
P
Model Fit
Anogenital Swab
HSV DNA log10 copy number / mL transport medium
Time after shedding onset (days)

Supplementary Figure 3. The deterministic form of the model without CD8+ lymphocyte parameters achieves poor fit with empiric data from lesional swabs. A typical example of failed deterministic model curve fitting to mucosal HSV-2 shedding curves with daily serial quantitative PCRs performed on anogenital lesions. Actual patient quantitative PCR data from anogenital swabs (blue squares) performed during anogenital lesions, and deterministic model fit (red line).

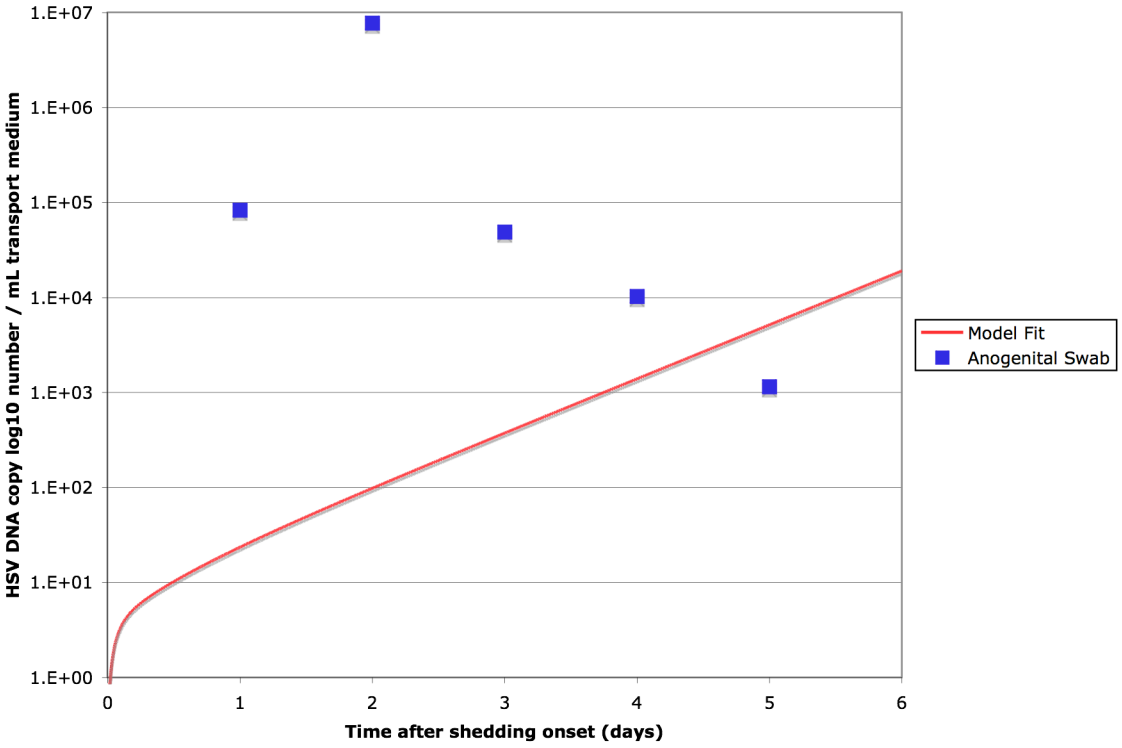

Supplementary Figure 4. The stochastic form of the model without CD8+ lymphocyte parameters leads to unrealistic shedding patterns with persistent viral shedding and epithelial cell infection. A stochastic simulation with the four-parameter model over thirty-days. Red line, log-10 HSV-2 DNA / mL. Green line, log-10 infected cells.

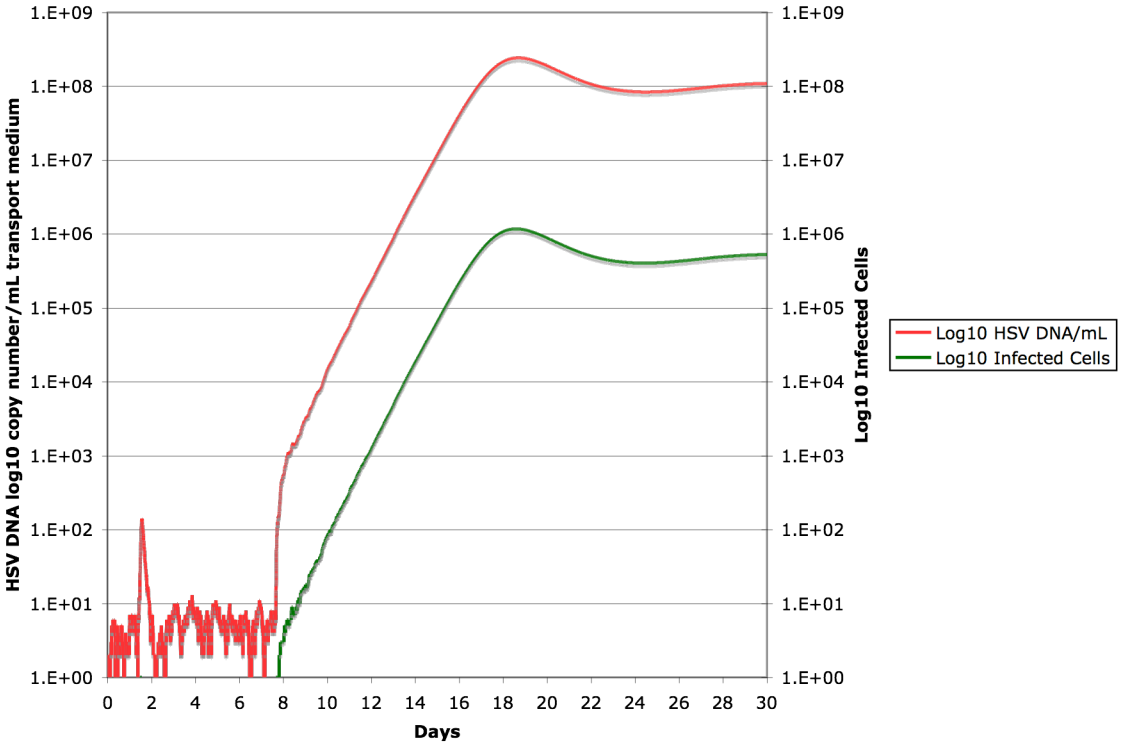

Supplementary Figure 5. High viral production precedes lesion detection. Kinetics of lesion formation, epithelial cell infection and viral production during a genital lesion according to a model simulation. (A) Instantaneous HSV copy number/mL transport medium (red line) and cumulative HSV copy number/mL transport medium (purple line) are shown on a log-10 scale (left y axis). Lesion diameter in millimeters is shown with a black line (right y axis). (B) Instantaneous number of infected cells (green line) and cumulative number of infected cells (orange line) are shown on a log-10 scale (left y axis). Lesion diameter in millimeters is shown with a black line (right y axis).

A

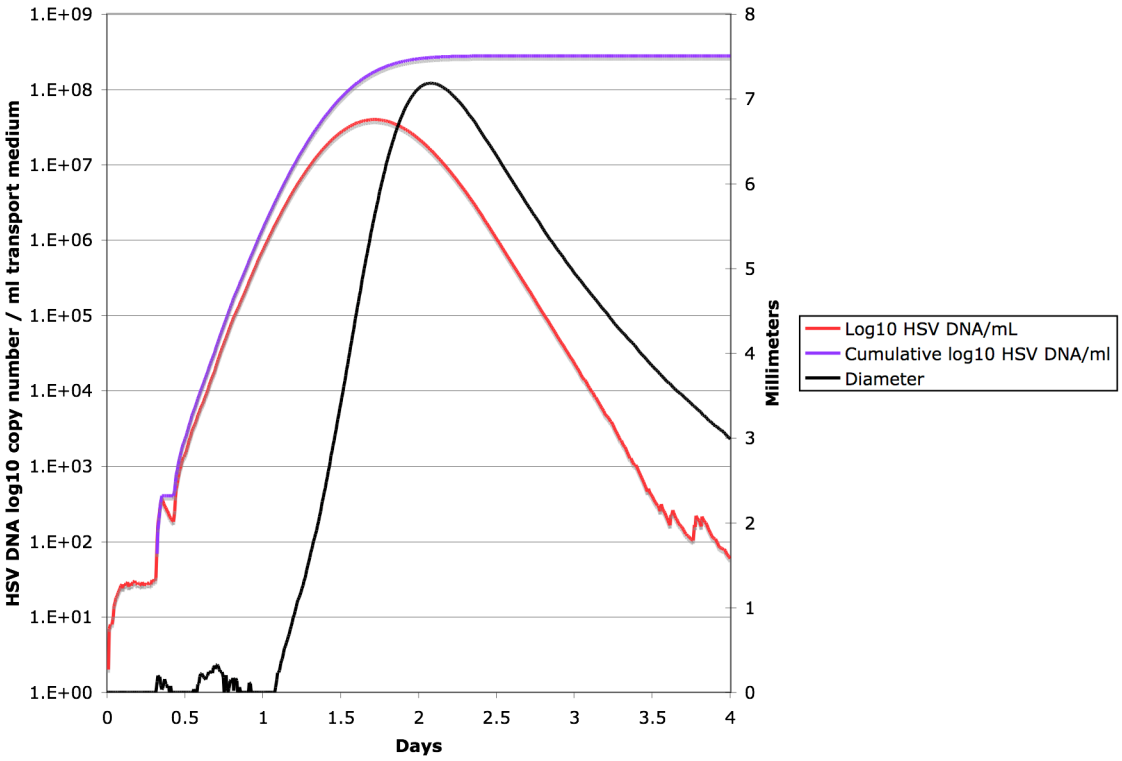

B

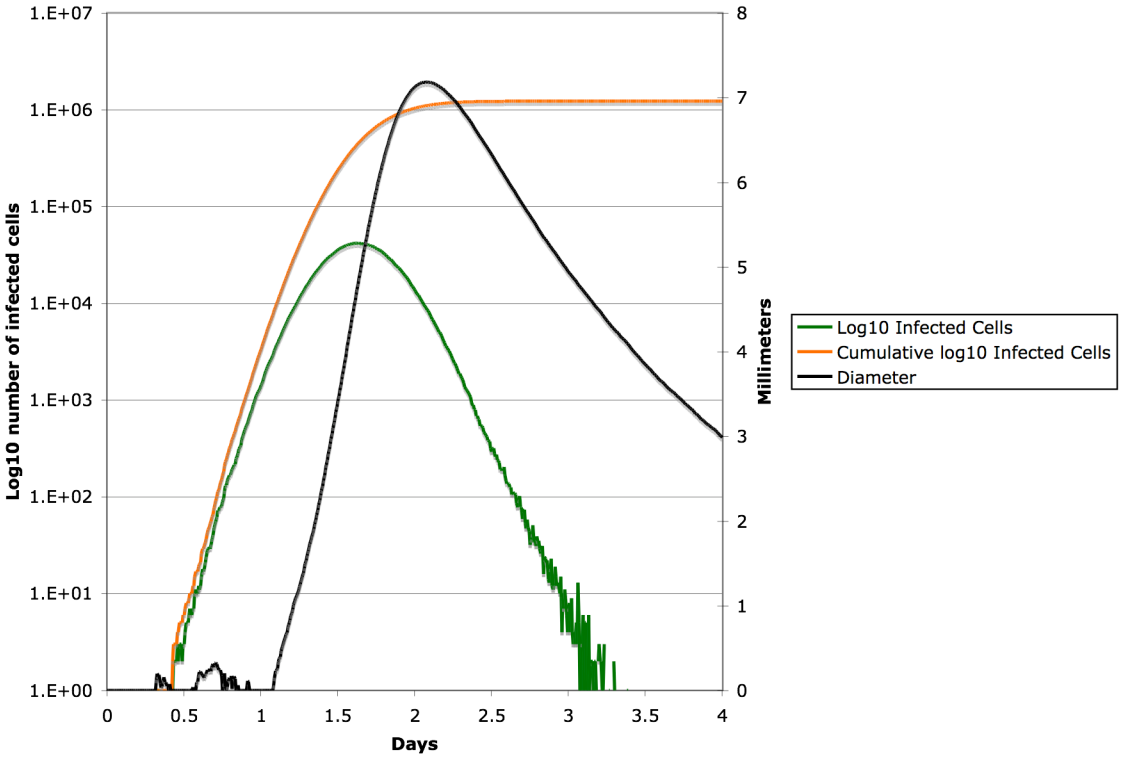
1.E+07
1.E+06
1.E+05
1.E+04
1.E+03
1.E+02
1.E+01
1.E+00
Log10 number of infected cells
0
0.5
1
1.5
2
2.5
3
3.5
4
Days
8
7
6
5
4
3
2
1
0
Millimeters
Log10 Infected Cells
Cumulative log10 Infected Cells
Diameter

Supplementary references

1. A. Wald, M. L. Huang, D. Carrell, S. Selke, L. Corey. Polymerase chain reaction for detection of herpes simplex virus (HSV) DNA on mucosal surfaces: comparison with HSV isolation in cell culture. *J Infect Dis* **188**,1345(2003).
2. K. E. Mark *et al.* Rapidly cleared episodes of herpes simplex virus reactivation in immunocompetent adults. *J Infect Dis* **198**,1141(2008).
3. A. Magaret, A. Wald, M. Huang, S. Selke, L. Corey. Optimizing PCR positivity criterion for detection of herpes simplex virus DNA on skin and mucosa. *J Clin Microbiol* **45**,1618(2007).
4. L. Corey, H. G. Adams, Z. A. Brown, K. K. Holmes. Genital herpes simplex virus infections: clinical manifestations, course, and complications. *Ann Intern Med* **98**,958(1983).
5. C. M. Crespi, W. G. Cumberland, A. Wald, L. Corey, S. Blower. Longitudinal study of herpes simplex virus type 2 infection using viral dynamic modelling. *Sex Transm Infect* **83**,359(2007).
6. J. Zhu *et al.* Persistence of HIV-1 receptor-positive cells after HSV-2 reactivation is a potential mechanism for increased HIV-1 acquisition. *Nat Med* **15**,886(2009).
7. J. Zhu *et al.* Virus-specific CD8+ T cells accumulate near sensory nerve endings in genital skin during subclinical HSV-2 reactivation. *J Exp Med* **204**,595(2007).
8. Euler. Institutionum calculi integralis Vol. Primum (1768). *Opera Omnia Series Prima* **11**,(1913).
9. H. M. Jaeger, S. R. Nagel. Physics of Granular States. *Science* **255**,1524(1992).
10. D. L. Chao, M. P. Davenport, S. Forrest, A. S. Perelson. A stochastic model of cytotoxic T cell responses. *J Theor Biol* **228**,227(2004).
11. S. S. Strand, T. K. Vanheyningen, D. A. Leib. The virion host shutoff protein of herpes simplex virus type 1 has RNA degradation activity in primary neurons. *J Virol* **78**,8400(2004).
12. K. D. Roizman B, in *Fields Virology,* H. P. Knipe DM, Griffin DE et al, Ed. (Lippincott Williams & Wilkins, Philadelphia, 2007).
13. R. J. De Boer, D. Homann, A. S. Perelson. Different dynamics of CD4+ and CD8+ T cell responses during and after acute lymphocytic choriomeningitis virus infection. *J Immunol* **171**,3928(2003).
14. V. V. Ganusov, R. J. De Boer. Estimating in vivo death rates of targets due to CD8 T-cell-mediated killing. *J Virol* **82**,11749(2008).
15. R. R. Regoes, A. Yates, R. Antia. Mathematical models of cytotoxic T-lymphocyte killing. *Immunol Cell Biol* **85**,274(2007).
16. R. R. Regoes, D. L. Barber, R. Ahmed, R. Antia. Estimation of the rate of killing by cytotoxic T lymphocytes in vivo. *Proc Natl Acad Sci U S A* **104**,1599(2007).
17. W. Barchet *et al.* Direct quantitation of rapid elimination of viral antigen-positive lymphocytes by antiviral CD8(+) T cells in vivo. *Eur J Immunol* **30**,1356(2000).
18. C. Jiang *et al.* Herpes simplex virus mutants with multiple substitutions affecting DNA binding of UL42 are impaired for viral replication and DNA synthesis. *J Virol* **81**,12077(2007).
19. C. Jiang, Y. T. Hwang, J. C. Randell, D. M. Coen, C. B. Hwang. Mutations that decrease DNA binding of the processivity factor of the herpes simplex virus DNA

polymerase reduce viral yield, alter the kinetics of viral DNA replication, and decrease the fidelity of DNA replication. *J Virol* **81**,3495(2007).

20. R. Turner, Z. Shehab, K. Osborne, J. O. Hendley. Shedding and survival of herpes simplex virus from 'fever blisters'. *Pediatrics* **70**,547(1982).